Earth's deep magma ocean never reached sulfide saturation

I. Blanchard, J. Siebert, E. Kubik, A. Minchenkova, L. Calvo, N. Wehr

Supplementary Information

The Supplementary Information includes:

- Methods and Data Selection
- Tables S-1 and S-2
- Figures S-1 and S-2
- Supplementary Information References

Methods

The objective of this work is to determine the amounts of sulfur that can be stored in the magma ocean at sulfur saturation. To this end, we performed a series of laser heated diamond anvil cell experiments at the putative P–T conditions of Earth's differentiation. We synthetized five samples between 53 and 72 GPa and 3800 to 4050 K. Following previous studies, the starting materials consisted of either a pyrolytic or a basaltic glass, both synthetized by aerodynamic levitation, subsequently polished down to a thickness of 20 microns, then machined into discs of 80-120 microns in diameter using a femto-second laser at Institut de Physique du Globe de Paris (IPGP, Blanchard *et al.*, 2017, 2022) . The metallic component was pure FeS powder. We used 200- to 300-microns cullet diamonds. For each run, we first pre-indented a 250-microns thick rhenium gasket to a thickness of about 50 microns, then drilled an experimental chamber of about 120 microns in diameter. FeS powder was subsequently loaded in between two silicate discs before starting compression. We controlled the pressure by using the Raman shift of the diamond anvil (Akahama and Kawamura, 2004). Once we reached the targeted pressure, we heated our samples for 10 to 120 seconds in IPGP, using a double-sided laser heating system. Temperature conditions and chosen time durations were such that both the sulfur and the silicate were

molten and closely approached chemical equilibrium, given the small size of our runs. The reported pressure was corrected for thermal pressure following Siebert *et al*., (2012).

The experiments were terminated by switching off the laser power, which results in extremely fast quench due to the high thermal conductivity of the diamonds. Experiments were subsequently slowly decompressed to atmospheric pressure, and the region of interest was extracted using Ga-Focused Ion Beam (FIB) facility at the GeoForschung Zentrum (GFZ) in Potsdam, Germany. Chemical analysis of sulfides and quenched melt were performed at IPGP using Scanning electron microscopy energy dispersive X-rays (EDX), equipped with a Field Emission Gun. Standards of FeS_2 were used for sulfur, wollastonite for Ca and Si, and pure Al_2O_3, MgO and NaCl for Al, Mg and Na respectively. Results are presented in Table S-1.

Oxygen fugacity calculation

We calculated the oxygen fugacity of our experiments relative to the iron-wüstite buffer (ΔIW). We have expressed the ideal oxygen fugacity of each of our runs following:

$$\Delta IW = 2\log\frac{X_{FeO}}{X_{Fe}} \quad \text{Eq. (S1)}$$

With X_{FeO} and X_{Fe} the mole fractions of FeO in the silicate and of Fe in the metal respectively. The assumption of ideal mixing in both phases is justified by the high temperatures of our runs, as done in previous experiments (e.g., Blanchard *et al*., 2017; Fischer *et al*., 2020; Huang *et al*., 2021).

Data selection

We explicitly excluded data for which the starting sulfide was not pure FeS (i.e., data containing Cu, Ni for instance), those with silicate compositions far from a pyrolytic composition (i.e., containing significant wt. % of TiO_2, H_2O and/or Na_2O), and experiments performed using graphite capsule. Importantly, data obtained in extremely reduced system with very low FeO content (<0.5 wt. %) were also excluded. This is because the influence of FeO at those conditions is not linear, and tends to a U-shaped curve (O'Neill and Mavrogenes, 2002). We have plotted on figure S-1 all the literature data used in our regression used along with the new ones from this study. We can see a clear effect of pressure, temperature, SiO_2 and FeO on SCSS. From this

figure, we can also see that the pressure domain has been extended by 20 GPa compared to previous experimental data, reaching now 72 GPa.

Comparison with data from Steenstra et al., 2022

Here, we report experimental results on SCSS at wider P-T conditions than previous studies with MORB-like silicate composition (Steenstra *et al*., 2022). We also observe that for similar FeO concentrations on the run products, SCSS derived by Steenstra *et al*., (2022) is lower than in our pyrolytic composition. The reproducibility between our single experiment with MORB-like starting material (SCSS4), and those of Steenstra *et al*., (2022), suggests that compositional factor on the silicate phase plays a significant role on sulfur storage on silicate melts. As observed in Wykes *et al*., (2014) and reported in Steenstra *et al*., (2022), we observe a correlation between SCSS-FeO, and SCSS-SiO_2, where pyrolite hosts more sulfur upon saturation. Given that SCSS increases with increasing FeO and decreasing SiO_2, we consider of importance to model it as a function of the composition of the silicate melt, which has not been performed previously (Steenstra *et al*., 2022). Through this approach, a model for predicting SCSS in a more realistic early Earth composition can be achieved.

Model of SCSS using only high P-T data

There is no experimental data between 23 and 43 GPa, which is a region where structural changes can occur, especially due to the increase of silicon coordination (Sanloup *et al*., 2013). Hence, we have also modelled the dependency of SCSS on P, T, X_{SiO2} and X_{FeO} using only data obtained at the putative conditions of core formation (i.e. > 30 GPa and > 3000 K). The only data that exist on this range are the ones presented in this study, along with the ones of (Steenstra *et al*., 2022), which makes only eight experimental data. We regressed those data with Eq. 2 presented in main text. We obtained the following regression, with uncertainties in brackets:

$$\ln S_{SCSS} = 10\ (0.5) - \frac{2959\ (2207)}{T} + 3.7(16)\frac{P}{T} + \frac{76\ 212\ (2861)}{T} \times X_{FeO} - \frac{25\ 333\ (4047)}{T} \times X_{SiO2} \quad \text{Eq. (S2)}$$

As can be seen, the pressure term is not relevant, so we did a second round of regression, excluding the pressure effect. By doing so, we obtain:

$$\ln S_{SCSS} = 10\ (0.5) - \frac{3327\ (1503)}{T} + \frac{7135\ (1908)}{T} \times X_{FeO} - \frac{25\ 695\ (3732)}{T} \times X_{SiO2} \quad \text{Eq. (S3)}$$

In this last regression (Eq. S3), the terms are evidently different from Eq. 2 (main text), but they display the same sign, and have smaller uncertainties.

Subsequently, we have included this regression in a model of magma ocean, as we presented in the main text. As can be seen in Fig. S-4, the evolution of SCSS over the course of accretion is different from the one presented in the main text and in Fig. 3, but the message holds. Indeed, regardless of the redox path, we still see that SCSS is way higher than the amount of sulfur present in the mantle due to core-mantle differentiation.

Supplementary Tables

Table S-1 Compositions of the experimental run products

Run #	SCSS1		SCSS2		SCSS3		SCSS4		SCSS5	
Silicate wt. %	N=8		N=13		N=9		N=16		N=13	
MgO	36.38	0.32	36.00	0.53	39.83	0.2	10.35	0.13	36.17	0.42
Al_2O_3	6.69	0.15	5.92	0.22	5.99	0.11	21.45	0.42	5.71	0.26
SiO_2	37.53	0.86	37.65	0.89	39.18	0.30	39.66	1.89	40.27	0.67
CaO	4.24	0.10	3.97	0.10	3.87	0.08	5.64	0.30	4.30	0.08
FeO	14.14	0.88	15.33	1.15	9.98	0.40	19.29	1.34	12.63	1.01
Na_2O	-	-	-	-	-	-	2.79	0.05	-	-
S	1.02	0.27	1.12	0.36	1.15	0.15	0.83	0.31	0.93	0.25
Total	100		100		100		100		100	
sulfide wt. %	N=6		N=5		N=4		N=7		N=7	
O	6.92	0.27	7.17	0.78	5.80	0.80	9.76	0.41	5.82	0.64
Mg	0.80	0.19	0.74	0.15	1.04	0.32	0.18	0.10	0.66	0.15
Al	0.21	0.02	0.23	0.02	0.27	0.07	0.34	0.09	0.18	0.07
Si	0.64	0.13	0.69	0.10	1.17	0.21	1.06	0.12	0.58	0.16
S	28.27	0.42	25.51	0.39	28.15	0.57	26.86	0.36	28.80	0.70
Fe	63.17	0.28	65.66	0.70	63.57	0.85	61.80	0.40	63.96	0.47
Total	100		100		100		100		100	

Table S-2 Compilation of experimental runs used in this study**,** is available for download (.xlsx) from the online version of this article.

Supplementary Figures

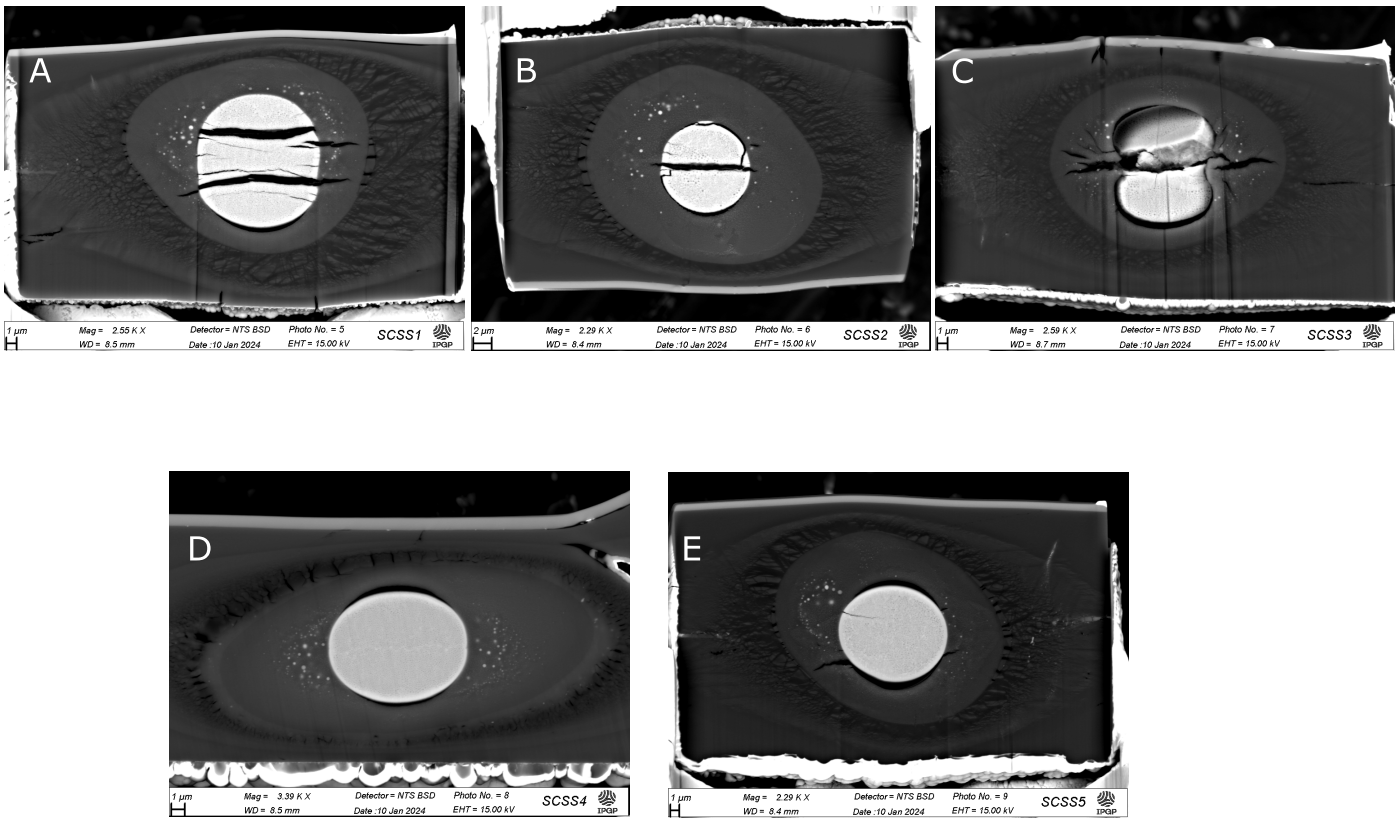

Figure S-1 Backscattered images of all our samples. A) SCSS1 synthesised at 64 GPa, 4000 K, B) SCSS2 synthesised at 61 GPa, 4000 K, C) SCSS3 synthesised at 72 GPa, 4050 K, D) SCSS4 synthesised at 53 GPa, 3800 K and E) SCSS5 synthesised at 53 GPa and 3800 K.

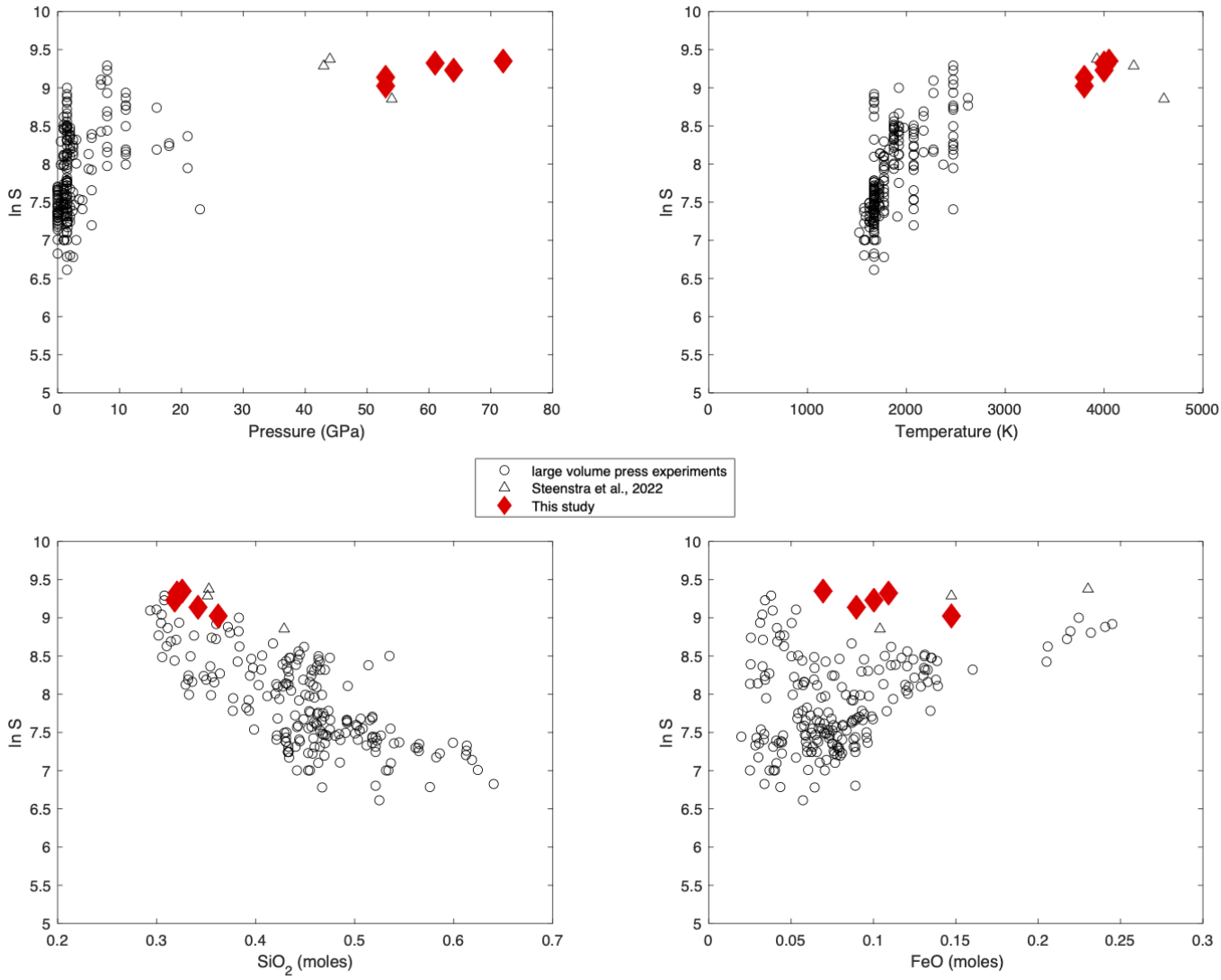

Figure S-2 Evolution of SCSS as a function of pressure, temperature, SiO_2 and FeO. Data labelled as large volume press experiments are from Wendlandt (1982); Mavrogenes and O'Neill (1999); O'Neill and Mavrogenes (2002); Holzheid and Grove (2002); Jugo *et al*., (2005); Liu *et al*., (2007); Kiseeva and Wood (2013); Ding *et al*., (2014); Wohlers and Wood (2015); Wood and Kiseeva (2015); Laurenz *et al*., (2016); Smythe *et al*., (2017); Blanchard *et al*., (2021).

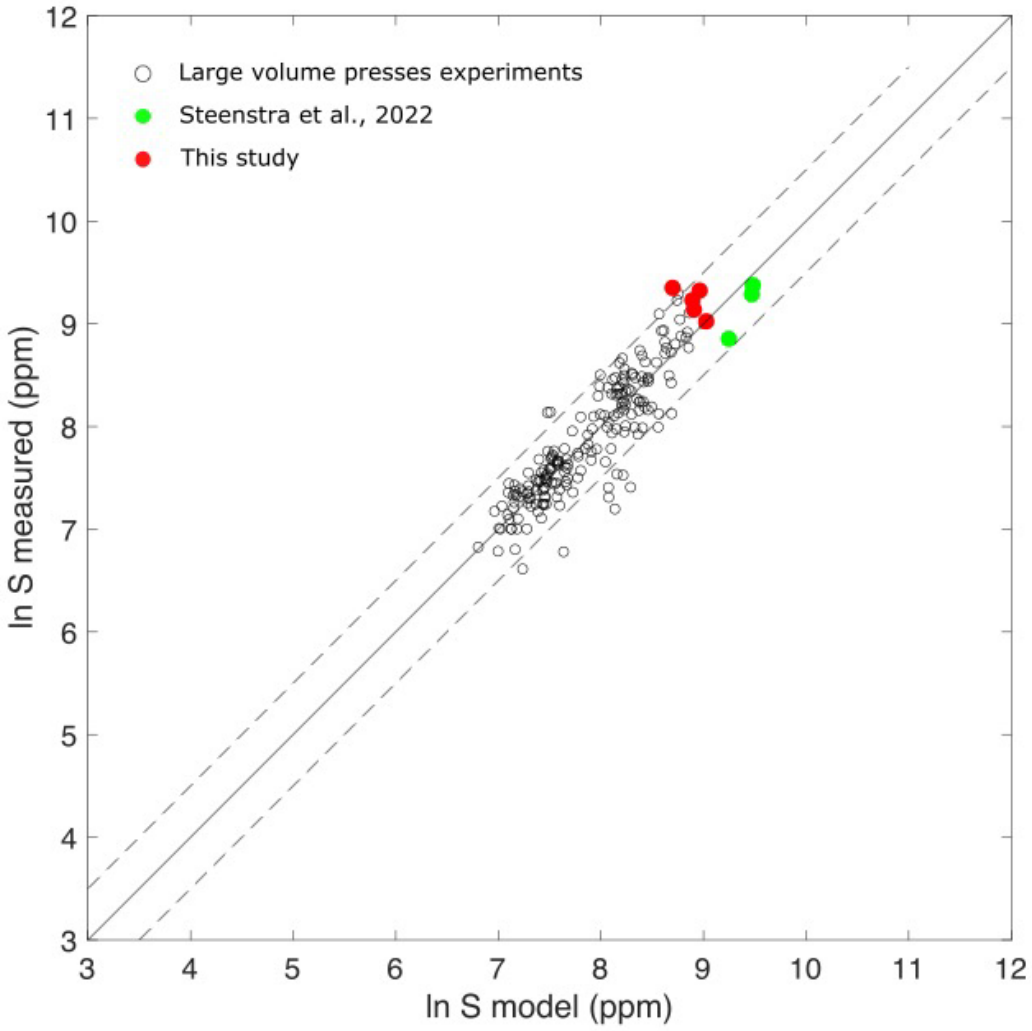

Figure S-3 Comparison between experimental data and results from our model (Eq. 2). Data from large volume presses experiments are from Wendlandt (1982); Mavrogenes and O'Neill (1999); O'Neill and Mavrogenes (2002); Holzheid and Grove (2002); Jugo *et al*., (2005); Liu *et al*., (2007); Kiseeva and Wood (2013); Ding *et al*., (2014); Wohlers and Wood (2015); Wood and Kiseeva (2015); Laurenz *et al*., (2016); Smythe *et al*., (2017); Blanchard *et al*., (2021).

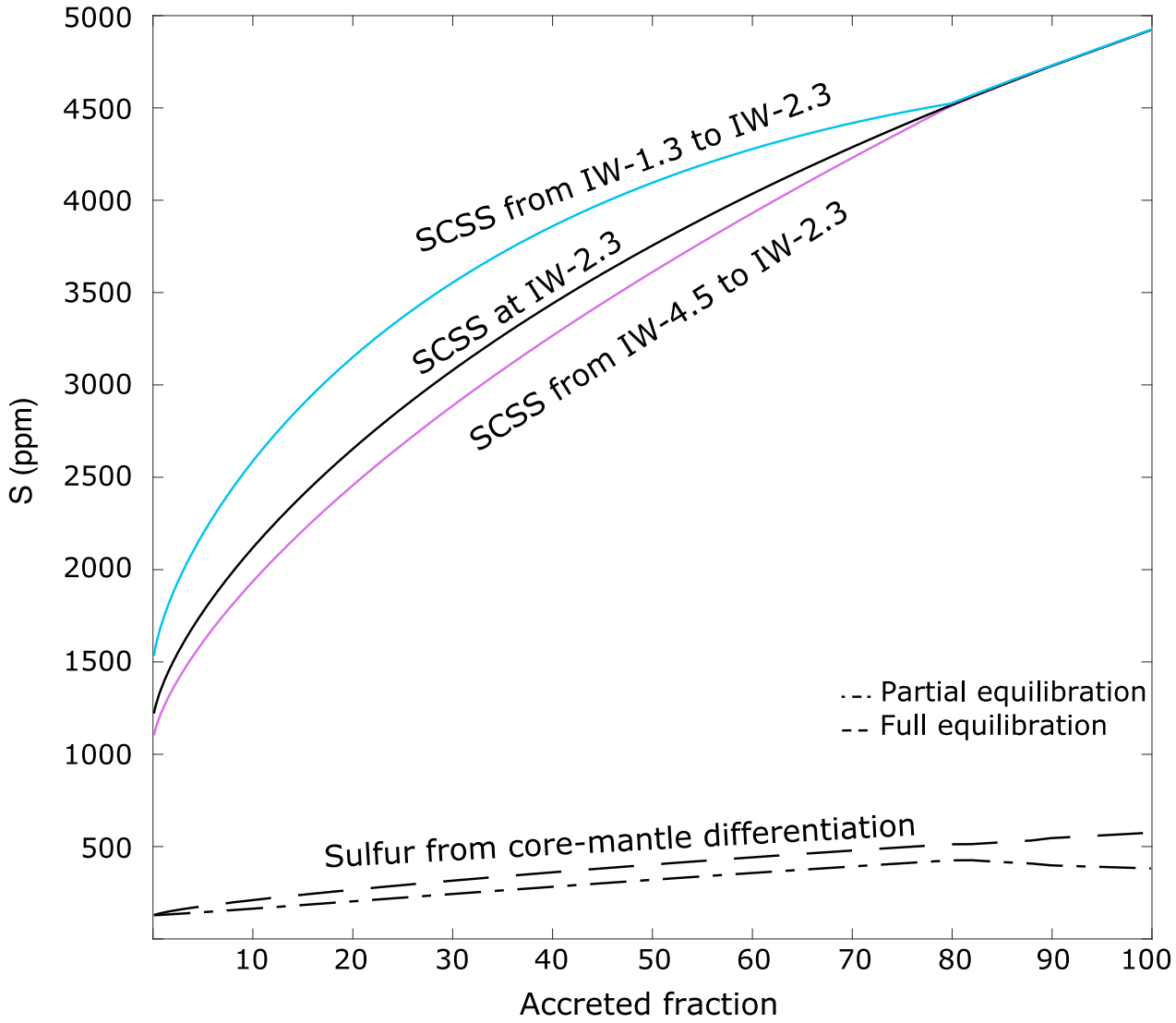

Figure S-4 Evolution of SCSS determined from Eq. S3, using only data obtained by diamond anvil-cell coupled with laser heating system (this study, Steenstra *et al*., 2022). Sulfur from core-mantle differentiation is calculated using Suer *et al*., (2017) model.

Supplementary Information References

Akahama, Y., Kawamura, H. (2004) High-pressure Raman spectroscopy of diamond anvils to 250 GPa: Method for pressure determination in the multimegabar pressure range. *Journal of Applied Physics* 96, 3748–3751.

Blanchard, I., Siebert, J., Borensztajn, S., Badro, J. (2017) The solubility of heat-producing elements in Earth's core. *Geochemical Perspectives Letters 5*, 1–5. https://doi.org/10.7185/geochemlet.1737

Blanchard, I., Abeykoon, S., Frost, D.J., Rubie, D.C. (2021) Sulfur content at sulfide saturation of peridotitic melt at upper mantle conditions. *American Mineralogist* 106, 1835–1843. https://doi.org/10.2138/am-2021-7649

Blanchard, I., Rubie, D.C., Jennings, E.S., Franchi, I.A., Zhao, X., Petitgirard, S., Miyajima, N., Jacobson, S.A., Morbidelli, A. (2022) The metal–silicate partitioning of carbon during Earth's accretion and its distribution in the early solar system. *Earth and Planetary Science Letters* 580, 117374. https://doi.org/10.1016/j.epsl.2022.117374

Ding, S., Dasgupta, R., Tsuno, K. (2014) Sulfur concentration of martian basalts at sulfide saturation at high pressures and temperatures - Implications for deep sulfur cycle on Mars. *Geochimica Cosmochimica Acta* 131, 227–246. https://doi.org/10.1016/j.gca.2014.02.003

Fischer, R.A., Cottrell, E., Hauri, E., Lee, K.K.M., Le Voyer, M. (2020) The carbon content of Earth and its core. *Proceedings of the National Academy of Sciences* 117, 8743–8749. https://doi.org/10.1073/pnas.1919930117

Holzheid, A., Grove, T.L. (2002) Sulfur saturation limits in silicate melts and their implications for core formation scenarios for terrestrial planets. *American Mineralogist* 87, 227–237. https://doi.org/10.2138/am-2002-2-304

Huang, D., Siebert, J., Badro, J. (2021) High pressure partitioning behavior of Mo and W and late sulfur delivery during Earth's core formation. *Geochimica Cosmochimica Acta* 310, 19–31. https://doi.org/10.1016/j.gca.2021.06.031

Jugo, P.J., Luth, R.W., Richards, J.P. (2005) An Experimental Study of the Sulfur Content in Basaltic Melts Saturated with Immiscible Sulfide or Sulfate Liquids at 1300 C and 1 GPa. *Journal of Petrology* 46, 783–798. https://doi.org/10.1093/petrology/egh097

Kiseeva, E.S., Wood, B.J. (2013) A simple model for chalcophile element partitioning between sulphide and silicate liquids with geochemical applications. *Earth and Planetary Science Letters* 383, 68–81. https://doi.org/10.1016/j.epsl.2013.09.034

Laurenz, V., Rubie, D.C., Frost, D.J., Vogel, A.K. (2016) The importance of sulfur for the behavior of highly-siderophile elements during Earth's differentiation. *Geochimica Cosmochimica Acta* 194, 123–138. https://doi.org/10.1016/j.gca.2016.08.012

Liu, Y., Samaha, N., Baker, D.R. (2007) Sulfur concentration at sulfide saturation (SCSS) in magmatic silicate melts. *Geochimica Cosmochimica Acta* 71, 1783–1799. https://doi.org/10.1016/j.gca.2007.01.004

Mavrogenes, J.A., O'Neill, H.S.C. (1999) The relative effects of pressure, temperature and oxygen fugacity on the solubility of sulfide in mafic magmas. *Geochimica Cosmochimica Acta* 63, 1173–1180. https://doi.org/10.1016/S0016-7037(98)00289-0

O'Neill, H.S.C., Mavrogenes, J.A. (2002) The Sulfide Capacity and the Sulfur Content at Sulfide Saturation of Silicate Melts at 1400°C and 1 bar. *Journal of Petrology* 43, 1049–1087. https://doi.org/10.1093/petrology/43.6.1049

Sanloup, C., Drewitt, J.W.E., Konôpková, Z., Dalladay-Simpson, P., Morton, D.M., Rai, N., Van Westrenen, W., Morgenroth, W. (2013) Structural change in molten basalt at deep mantle conditions. *Nature* 503, 104–107. https://doi.org/10.1038/nature12668

Siebert, J., Badro, J., Antonangeli, D., Ryerson, F.J. (2012) Metal–silicate partitioning of Ni and Co in a deep magma ocean. *Earth and Planetary Science Letters* 321–322, 189–197. https://doi.org/10.1016/j.epsl.2012.01.013

Smythe, D.J., Wood, B.J., Kiseeva, E.S. (2017) The S content of silicate melts at sulfide saturation: New experiments and a model incorporating the effects of sulfide composition. *American Mineralogist* 102, 795–803. https://doi.org/10.2138/am-2017-5800CCBY

Steenstra, E.S., Lord, O.T., Vitale, S., Bullock, E.S., Klemme, S., Walter, M. (2022) Sulfur solubility in a deep magma ocean and implications for the deep sulfur cycle. *Geochemical Perspectives Letters* 22, 5–9. https://doi.org/10.7185/geochemlet.2219

Suer, T.A., Siebert, J., Remusat, L., Menguy, N., Fiquet, G. (2017) A sulfur-poor terrestrial core inferred from metal–silicate partitioning experiments. *Earth and Planetary Science Letters* 469, 84–97. https://doi.org/10.1016/j.epsl.2017.04.016

Wendlandt, R.F. (1982) Sulfide saturation of basalt and andesite melts at high pressures and temperatures. *American Mineralogist* 67, 877–885.

Wohlers, A., Wood, B.J. (2015) A Mercury-like component of early Earth yields uranium in the core and high mantle ^{142}Nd. *Nature* 520, 337–340. https://doi.org/10.1038/nature14350

Wood, B.J., Kiseeva, E.S. (2015) Trace element partitioning into sulfide: How lithophile elements become chalcophile and vice versa. *American Mineralogist* 100, 2371–2379. https://doi.org/10.2138/am-2015-5358ccbyncnd

Wykes, J.L., O'Neill, H.S.C., Mavrogenes, J.A. (2014) The effect of FeO on the sulfur content at sulfide saturation (SCSS) and the selenium content at selenide saturation of silicate melts. *Journal of Petrology* 56, 1407–1424. https://doi.org/10.1093/petrology/egv041